Volume 1 | Number 1 | Jan 2013 | Pages 1–100

ChemComm

Chemical Communications
www.rsc.org/chemcomm

ROYAL SOCIETY OF CHEMISTRY

This is an *Accepted Manuscript*, which has been through the Royal Society of Chemistry peer review process and has been accepted for publication.

Accepted Manuscripts are published online shortly after acceptance, before technical editing, formatting and proof reading. Using this free service, authors can make their results available to the community, in citable form, before we publish the edited article. We will replace this *Accepted Manuscript* with the edited and formatted *Advance Article* as soon as it is available.

You can find more information about *Accepted Manuscripts* in the **Information for Authors**.

Please note that technical editing may introduce minor changes to the text and/or graphics, which may alter content. The journal's standard **Terms & Conditions** and the **Ethical guidelines** still apply. In no event shall the Royal Society of Chemistry be held responsible for any errors or omissions in this *Accepted Manuscript* or any consequences arising from the use of any information it contains.

ChemComm

COMMUNICATION

In situ atomic scale visualization of surface kinetics driven dynamics of oxide growth on Ni-Cr surface

Langli Luo[a], Lianfeng Zou[b], Daniel K. Schreiber[c], Matthew J. Olszta[c], Donald R. Baer[a], Stephen M. Bruemmer[c], Guangwen Zhou*[b], and Chong-Min Wang*[a]

We report in situ atomic-scale visualization of the dynamical three-dimensional growth of NiO during initial oxidation of Ni-10at%Cr using environmental transmission electron microscopy. Step-by-step adatom growth mechanism in 3D is observed and change of surface planes of growing oxide islands can be induced by local surface kinetic variations.

The interaction of oxygen with alloy surfaces is of great interest to a wide range of technological applications including passivation of metals[1-3], heterogeneous catalysis[4-6] and failure of semiconductor devices[7,8]. However, many fundamental questions persist especially in the initial stages of oxidation. Among them, the atomic mechanism underlying the 3D growth of oxide islands beyond a few layers is largely unknown although surface science studies have provided tremendous information on oxygen adsorption induced metal surface reconstructions[9-11]. The early stages of metal oxidation generally involve the nucleation and growth of 3D oxide islands before steady-state oxidation begins[12-16]. Early oxidation stages for alloys are complicated by the nucleation and growth of different oxide phases, where more than one element can be oxidized simultaneously.[17,18] From the practical point of view, the early-stage oxidation behavior can exert a strong influence on the microstructure evolution of the oxide film in the later stages of the oxidation and thus the kinetics of the steady-state oxidation.

Step-edge induced oxide growth as a result of direct interaction of oxygen gas and the metal surface has been reported on Cu surfaces[19]. Different from the long-held oxidation model of the solid-solid transformation[20-24], the presence of surface steps facilitates oxide formation without involving oxygen subsurface incorporation. The initial oxide film can grow from a 2D wetting-layer to 3D islands by overcoming a critical thickness, which is similar to the Stranski-Krastanov (SK) mode of thin film growth[25,26]. The 3D islands with a thickness of a few atomic layers are usually not well faceted while several compact island shapes – including squares, triangles, hexagons and round shapes – are prevalently found during the early stages of metal and alloy oxidation[13]. To understand how these different shapes have developed, we need to know the underlying mechanism for 3D oxide growth. Ni-Cr is a model alloy system for developing oxidation-resistive alloys.[27] Since both Ni and Cr can be oxidized, the growth of initial oxides is of great importance in determining the microstructure of the oxide scale toward effective passivation of the alloy. Herein, we employ *in situ* environmental transmission electron microscopy (ETEM) to monitor the initial oxide growth on a Ni-10at%Cr surface at atomic scale in real time. We observe that NiO crystals nucleate and grow epitaxially on the Ni-Cr surface first, and it proceeds through step-by-step adatom mechanisms sustained by surface diffusion of Ni and O atoms. The surface planes of the oxide islands can be changed upon surface kinetic variation. No Cr_2O_3 phase has been found during the initial oxidation process (~5min). These results demonstrate the surface diffusion determines the morphology and growth kinetics of oxide islands during initial oxidation of this Ni-Cr alloy.

The oxidation experiments were carried in an environmental TEM (FEI Titan® 80-300) equipped with an objective-lens aberration corrector. The single crystal Ni-10at%Cr (100) thin film of ~ 40 nm was grown on a NaCl (100) substrate by e-beam evaporation. The alloy film was removed from the substrate by suspending in the deionized water, then washed (in acetone and methanol) and mounted on the TEM grid. The Ni-Cr films were annealed using the Gatan® 652 double-tilt heating holder at 450°C with the flow of H_2 gas to remove native oxides. *In situ* TEM observations were made in both planar view on (100) surface and cross-sectional view on <110> edges of the Ni-10at%Cr (100) film oxidized at 450°C at an oxygen partial pressure $pO_2 = 3 \times 10^{-6}$ mbar unless otherwise specified.

Figure 1A-C depicts the general process of oxide growth on the Ni-10at%Cr (100) film for the first few minutes, which proceeds through oxide islanding along the film edges and on the film surface. Immediately after introducing the oxygen gas, oxide

a. *Environmental Molecular Sciences Laboratory, Pacific Northwest National Laboratory, Richland, WA 99352, USA.*
b. *Department of Mechanical Engineering & Multidisciplinary Program in Materials Science and Engineering, State University of New York, Binghamton, NY13902, USA.*
c. *Energy and Environment Directorate, Pacific Northwest National Laboratory, Richland, WA 99352, USA.*

† Electronic Supplementary Information (ESI) available: For ESI and *in situ* videos see DOI: 10.1039/x0xx00000x
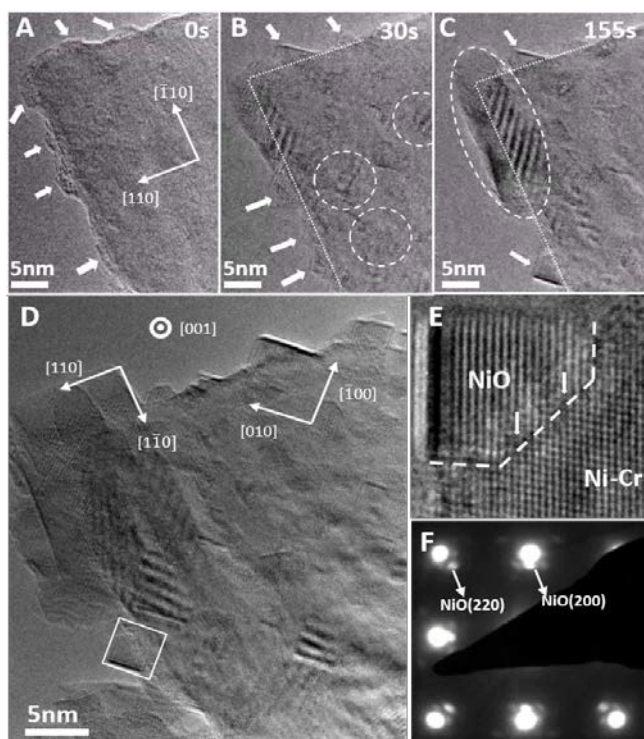
COMMUNICATION

Fig. 1 (A)-(C) *In situ* TEM images of nucleation and growth of NiO on two <110> edges of Ni-10at%Cr (100) during the oxidation at 450°C and pO$_2$=3×10^{-6}mbar (see in situ TEM movie S1 in the supplementary materials). (D) Oxidized alloy surface after 363s shows cubic oxide islands exposing only <100> or <110> surfaces. (E) HRTEM image of enlarged area from (D) shows epitaxial relation between oxide and alloy substrate, the interface is indicated as white dotted line and white arrows show two dislocations. (F) Selected-area electron diffraction pattern of the oxidized alloy surface shows epitaxial relation between oxide and alloy.

nucleation occurs along the two <011> edges of the alloy film indicated by arrows in Fig. 1A. These initial oxide films do not show strong diffraction contrast of lattices, indicating that they may not have well-ordered crystal structures as adjacent alloy film. They can experience oscillatory growth due to the presence of surface steps leading to metastable atomic structures[28]. With continued oxidation, all of the edge-on oxide (white arrows) grows into stable 3D oxide with clear facets after 30 s, as seen in Fig. 1B. Simultaneously, oxidation proceeds along the entire planar surface area of the alloy film, as evidenced by the Moiré fringes (dashed-line circles) caused by overlapping NiO and Ni-Cr lattices. After 155 s, the lateral dimensions of the NiO oxide reach 5 nm and the corner oxide island (dashed-line ellipse) with <110> surface planes have outgrown the other two oxide islands with <100> surface planes (up and bottom arrows) seen in Fig. 1C. The edges of the alloy sample are indicated by white-dash lines in Fig. 1B and C. Fig. 1D shows a high-resolution (HR) TEM image of this Ni-10at%Cr (100) thin film oxidized for 363s. It can be seen that two <110> edges and the planar surface area of the film are fully covered with several NiO islands with either (100) or (011) surfaces. The enlarged HRTEM image in Fig. 1E shows a NiO island grown on the Ni-Cr (011) surface with an epitaxial relationship of (001)NiO ∥ (001)Ni-Cr and [011]NiO ∥ [011]Ni-Cr. The interface between the NiO island and the metal alloy substrate is depicted by a white dotted line, and two white arrows indicate the locations of misfit dislocations caused by their lattice mismatch. The NiO phase and cube-on-cube epitaxy were further confirmed by the selected-area electron diffraction (SAED) pattern in Fig. 1F. No additional reflections from other oxide
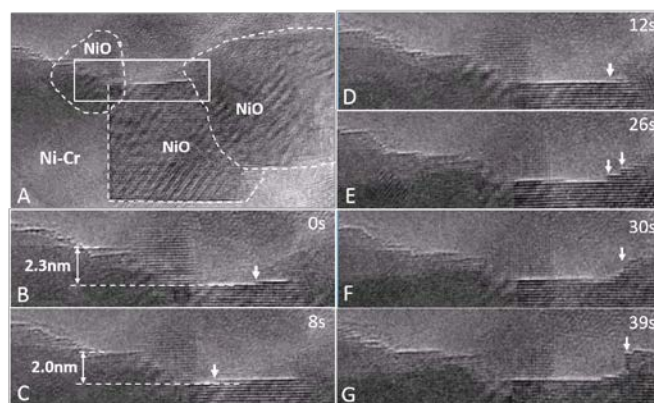

Fig. 1 (A) HRTEM image of three NiO islands grown on Ni-10at%Cr (100) during the oxidation at 450°C and pO$_2$=3×10^{-6}mbar. (B)-(G) Time-resolved HRTEM images of NiO islands growth under the above conditions (see in situ TEM movie S2 in the supplementary materials)

phases (e.g. NiCr$_2$O$_4$ or Cr$_2$O$_3$) were observed and the additional satellite spots are caused by double-diffraction. Although it is possible that Cr forms oxides without well-ordered crystal structures resulting no diffraction spots in SAED pattern, all of the oxide islands emerged on the alloy surface show epitaxial NiO phase in Fig. 1D. Cross-sectional TEM imaging of a similar sample with longer oxidation time revealed Cr-rich oxide at the interface between outward growing NiO and metal alloy, suggesting that Cr is also oxidized but does not inhibit NiO formation in this initial stage. This delayed formation of Cr-based oxides has been reported for both Fe-Cr and Ni-Cr alloys[2], i.e., the alloys with lower concentration (<15%) Cr show no Cr$_2$O$_3$ phase in the first a few minutes while the Cr$_2$O$_3$ phase is always present in the alloy with higher (~30%) Cr concentration. The absence of Cr-based oxides during initial oxidation of alloy with low Cr concentration is largely due to that the kinetically favored NiO formation consumed all the oxygen atoms on the surface in our test conditions resulting in tracer amount or no Cr based oxide formation. From these observations, it is apparent that the initial oxidation of Ni-Cr film is dominated by the epitaxial growth of NiO rather than Cr oxide. As the oxide islands growth continues, cubic island morphologies develop along the alloy surface. The 3D growth of oxide islands results from the increasing strain energy caused by lattice mismatch between NiO and Ni-Cr in the system. According to the Vegard's law, for solid solution Ni-10at%Cr alloy with the same face-centered cubic (fcc) structure as pure Ni, the lattice constant is calculated as $a_{Ni-10at\%Cr} = (1 - 0.1)a_{Ni} + 0.1a_{Cr}$=3.456Å. The natural lattice misfit, $f = (a_{NiO} - a_{Ni-10at\%Cr})/a_{NiO}$, between Ni-Cr and NiO is ~17.1%. As seen in Fig. 1E, this large lattice misfit is accommodated by the presence of misfit dislocations, i.e., dislocations appear every 6 atomic layers of NiO lattice, which results in reduced lattice mismatch between the oxide and alloy substrate. The measured lattice misfit between Ni-Cr (measured as 3.514 Å) and NiO (measured as 4.02 Å) is ~ 14.3%. Although the grown NiO is still strained by ~2% comparing with the natural lattice space of NiO ~4.17 Å, the relaxation of large lattice misfit makes the 3D growth of oxide islands is thermodynamically favourable over 2D epitaxial layer growth because the reduction in the epitaxial strain energy outweighs the increase in island surface energy.

Figure 2 depicts the dynamic atomistic process of NiO island growth on the Ni-Cr (100) surface through a series of time-resolved HRTEM images. In Fig. 2A, three oxide islands are present on the Ni-Cr (100) surface as shown clearly by the moiré fringes. The following

images in Fig. 2B to G focus on the [100] edge of the oxide island located at the center (indicated by the white box in Fig.2A). The *in situ* TEM images show that the oxide grows through a layer-by-layer mode by consuming the adjacent stepped alloy surface. Initially, the growth front of the new oxide layer (indicated by the white arrow in Fig. 2B) propagates from the right to the left side. After 8 s (Fig. 2C), it has grown ~ 3.1 nm laterally, corresponding to ~15 atomic columns (the lattice distance for NiO (200) planes is 2.08Å) shown in Fig. 2C. At the same time, the upper terrace of the stepped alloy surface on the left decreases its height from 2.3 nm to 2.0 nm indicating Ni atoms in this region are consumed for the oxide growth, possibly through atom detachment from the stepped surface. Within another 4 s, a second oxide layer has grown as seen in Fig. 2D. These *in situ* TEM images clearly show that the oxide island grows layer by layer via an adatom process, which involves the preferential formation of new oxide at the step-edge and the step-edge moves laterally as the oxidation proceeds. It is natural to expect that step edges are thermodynamically favoured sites for oxide formation because they lower the system free energy. But it is also noted that because Ni atoms have to diffuse to the reaction front on the oxide surface to grow oxide layer, the upper terrace has shorter diffusion length comparing with lower terrace, which makes it possible to nucleate new oxide on the upper terrace. The interplay of thermodynamic and kinetic factors results in the growth of new oxide on both upper and lower terrace but the oxide on upper terrace is always limited by the step-edges as illustrated in Fig. 2E to G, wherein the new oxide layers (indicated by arrows) on the upper terrace cannot cross the existing step-edge leading to the formation of two-atomic-layer and even four-atomic-layer high steps during the oxide growth. This has been observed previously[28] for the oxide formation on Cu surfaces, which is due to oxygen adsorption on the lower terrace along the step-edge, destabilizing the oxide layer formed on the upper terrace. It is also noted that an additional oxide layer propagates from the left to right and meets with the growth front of an existing oxide layer in Fig. 2F, which indicates the new oxide growth on the lower terrace is possible and follows the adatom growth mode.

The layer-by-layer adatom growth mode of oxide islands observed above requires fast surface diffusion of Ni and O atoms to the step-edge growth front. When the dimensions of oxide islands are small and the alloy surface is not fully covered with oxides, the diffusion of Ni atoms over the surface of oxide islands is kinetically more favorable that than bulk diffusion through oxide islands. While O molecules directly impinge, dissociate and diffuse on the entire sample surface, the consumption of Ni atoms from the alloy was observed directly through the decreasing step height and changing step edges as seen in Fig.2. Further evidence on a larger length scale can be in time-resolved bright-field TEM images in the supplemental Fig. S1. The increasing area of white contrast with oxidation time clearly shows that the consumption of Ni-Cr alloy during oxidation proceeds in a fashion of layer-by-layer peeling of atoms along <100> directions. Taken together, these observations clearly demonstrate that the initial oxidation of Ni-10at%Cr is dominated by surface diffusion of Ni and O atoms.

The equilibrium shapes of crystals are usually related to their surface energies and can be determined by Wulff constructions. The oxidation of metals is a "non-equilibrium" process, which can be a kinetics-dominated process as shown above. Hence, the shapes of the growing oxide islands can be dynamic and sensitive to the changes in kinetic conditions. This metastability is illustrated for NiO by a transition of surface planes from the (100) to (110) surfaces on a small oxide island as seen in a series of time-resolved

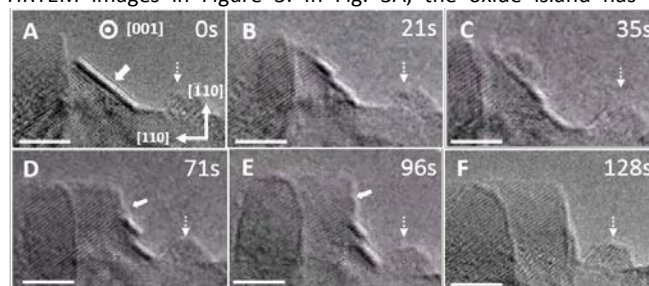HRTEM images in Figure 3. In Fig. 3A, the oxide island has an

Fig. 3 (A)-(E) Time-resolved HRTEM images of the (100) surface of one NiO island grown on Ni-10at%Cr (100) during the oxidation at 450°C and pO$_2$=3×10^{-6}mbar, depicting a transition from (100) to (110) surface of the NiO island. The scale bar is 5nm.

exposed edge-on (100) surface plane as indicated by the solid white arrow. With time new oxide layers grew from the top-left to the bottom-right of the (100) plane until intersecting the alloy surface. Two step-edges are clearly visible in Fig. 3B after 21 s, indicating that a few atomic layers of oxide have grown onto the NiO (100). Rather than layer-by-layer growth observed in Fig. 2, the large step height (1-2 nm) here indicates that the step consists of multiple atomic layers. Therefore the propagation of a single-layer step-edge is much slower than the formation of new oxide layers on the upper terrace. At the same time, the upper-most oxide layer consistently stops growing at the step-edges, resulting in the formation of a dome-like new island seen in Fig. 3C. By accumulating new oxide layers on the (100) surface, which are limited by steps, a new (110) surface plane is partially formed where many step-edges meet as seen in Fig. 2D. This new (110) plane meets the pre-existing (100) step resulting in a new step-edge with a 135° slope, which becomes the new growth front of the oxide layer. In Fig. 3D and 3E, the new oxide layer grows from the new step-edge to the far end of the new (110) surface as evidenced by the advancing of a step-edge indicated by the white arrows. Through this atomistic route, the new (110) surface plane has completely replaced the original (100) surface plane after 128 s of oxidation. This transition of the growing surface planes of the oxide island may stem from locally inhibited diffusion on (100) surface of the oxide island along with the Ehrlich-Schwoebel (E-S) barrier[29, 30] inhibiting crossing the step-edge. As seen in Fig. 3, a growing NiO island indicated by the dashed-line arrow is visible on the right side of the central oxide island. As oxidation proceeds, this oxide island grows and approaches to the central oxide island, inhibiting the diffusion of Ni and O atoms nearby. This occurs because each oxide island acts as a sink for reacting species in a surface diffusion governed oxidation process.[12] Hence, the growth of two adjacent oxide islands inhibits surface diffusion of reacting species (Ni and O) in the area between them. Figure 4 shows the schematic of the (100) → (110) transition for the oxide surface caused by this local kinetic variation. Because of the inhibited surface diffusion of reacting species from lower terrace (right side), most of Ni atoms diffuse to the upper terrace from the left side (Fig. 4A). For a stepped surface, the E-S barrier is an additional diffusion barrier, encountered by a moving surface atom when crossing an atomic step since it has to pass through the area (steps) with a low number of nearest neighbors comparing with that on the terrace. Hence, Ni atoms have much larger chance to diffuse to the site 1 rather than cross the step-edge to site 2, resulting in the preferential formation of new oxide layers on the upper terrace rather than that on the lower terrace (Fig. 4B). While more oxide layers nucleate and grow on the upper layer, layer by layer, step-edges have been created through this process at the

ChemComm Accepted Manuscript

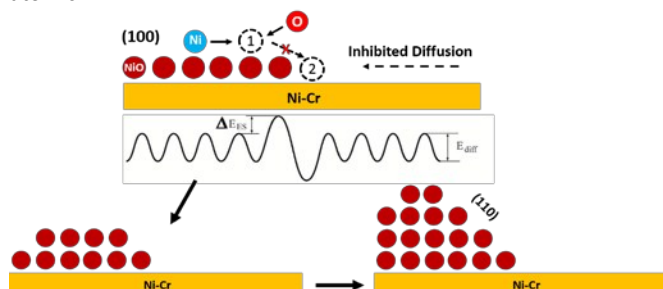same time. These step-edges brought even larger E-S barrier for atomic

Fig. 4 Schematic of the transition from (100) to (110) surfaces on a NiO island during the oxidation of Ni-10at%Cr alloy. A) Ni atom (blue) diffuses to site 1 to form NiO (brown) with O (red) on initial NiO layer but cannot diffuse to site 2 on lower terrace because of additional E-S barrier. B) More NiO layers formed on upper terrace leading to C) the transition from (100) to (110) surface of NiO. Note that the surface diffusion of Ni and O are inhibited from right indicated as dashed-line arrow because of the existence of another NiO island on the right (not shown here).

diffusion. Eventually, these step-edges line up to form the new (110) surface on the oxide island (Fig. 4C). This illustrates how the surface diffusion controls the growth morphology of oxide islands during initial oxidation of alloy.

In summary, we have observed the atomistic processes of the 3D growth of oxide islands during initial stages of Ni-10at%Cr alloy oxidation in real time. Our in situ TEM visualization reveals that the oxide growth generally proceeds through an adatom mechanism involving surface diffusion of Ni and O atoms to the growth front. This layer-by-layer growth mode can be altered by variation in local kinetics, i.e. limited surface diffusion in the area adjacent to the oxide island. This can lead to a transition from (100) to (110) surface planes of the oxide island, which can be understood through the effect of E-S barrier. Understandings of the detailed atomistic route for 3D growth of oxide islands on alloy surface not only provide insight to effective passivation of alloy surface but also have broader impact on controlling the growth of heterogeneous nanostructures on substrate.

Notes and references

1. D. L. Douglass, *Corrosion Science*, 1968, **8**, 665-678.
2. B. Chattopadhyay and G. C. Wood, *Journal of The Electrochemical Society*, 1970, **117**, 1163-1171.
3. G. Calvarin, R. Molins and A. M. Huntz, *Oxidation of Metals*, 2000, **53**, 25-48.
4. F. Besenbacher, I. Chorkendorff, B. S. Clausen, B. Hammer, A. M. Molenbroek, J. K. Nørskov and I. Stensgaard, *Science*, 1998, **279**, 1913-1915.
5. K.-W. Park, J.-H. Choi, B.-K. Kwon, S.-A. Lee, Y.-E. Sung, H.-Y. Ha, S.-A. Hong, H. Kim and A. Wieckowski, *The Journal of Physical Chemistry B*, 2002, **106**, 1869-1877.
6. E. Nikolla, J. Schwank and S. Linic, *Journal of Catalysis*, 2009, **263**, 220-227.
7. *United States Pat.*, 6100195, 2000.
8. N. L. Michael, C.-U. Kim, P. Gillespie and R. Augur, *Applied Physics Letters*, 2003, **83**, 1959-1961.
9. D. F. Mitchell, P. B. Sewell and M. Cohen, *Surface Science*, 1976, **61**, 355-376.
10. G. Allen, P. Tucker and R. Wild, *Oxidation of Metals*, 1979, **13**, 223-236.
11. S. M. Thurgate and P. J. Jennings, *Surface Science*, 1983, **131**, 309-320.
12. J. C. Yang, M. Yeadon, B. Kolasa and J. M. Gibson, *Applied Physics Letters*, 1997, **70**.
13. G. Zhou and J. C. Yang, *Applied Surface Science*, 2003, **210**, 165.
14. L. Wang and J. C. Yang, *Journal of Materials Research*, 2005, **20**, 1902-1909.
15. L. Luo, Y. Kang, J. C. Yang, D. Su, E. A. Stach and G. Zhou, *Applied Physics Letters*, 2014, **104**, 121601.
16. L. Luo, Y. Kang, J. C. Yang and G. Zhou, *Journal of Applied Physics*, 2015, **117**, 065305.
17. F. Gesmundo and B. Gleeson, *Oxidation of Metals*, 1995, **44**, 211-237.
18. M. P. Brady, I. G. Wright and B. Gleeson, *JOM*, 2000, **52**, 16-21.
19. G. Zhou, L. Luo, L. Li, J. Ciston, E. A. Stach and J. C. Yang, *Physical review letters*, 2012, **109**, 235502.
20. K. R. LAWLESS, *Rep. Prog. Phys.*, 1974, **37**, 231.
21. M. Todorova, W. X. Li, M. V. Ganduglia-Pirovano, C. Stampfl, K. Reuter and M. Scheffler, *Phys. Rev. Lett.*, 2002, **89**, 096103.
22. J. Gustafson, A. Mikkelsen, M. Borg, E. Lundgren, L. Köhler, G. Kresse, M. Schmid, P. Varga, J. Yuhara, X. Torrelles, C. Quirós and J. N. Andersen, *Phys. Rev. Lett.*, 2004, **92**, 126102.
23. M. Todorova, K. Reuter and M. Scheffler, *Phys. Rev. B*, 2005, **71**, 195403.
24. U. Starke, M. A. Van Hove and G. A. Somorjai, *Progress in Surface Science*, 1994, **46**, 305-319.
25. Y. W. Mo, D. E. Savage, B. S. Swartzentruber and M. G. Lagally, *Physical Review Letters*, 1990, **65**, 1020-1023.
26. G. Zhou, L. Luo, L. Li, J. Ciston, E. A. Stach, W. A. Saidi and J. C. JYang, *Chem. Commun.*, 2013, **49**, 10862-10864.
27. B. Chattopadhyay and G. C. Wood, *Oxidation of Metals*, 1970, **2**, 373-399.
28. L. Li, L. Luo, J. Ciston, W. A. Saidi, E. A. Stach, J. C. Yang and G. Zhou, *Physical Review Letters*, 2014, **113**, 136104.
29. R. L. Schwoebel and E. J. Shipsey, *Journal of Applied Physics*, 1966, **37**, 3682-3686.
30. R. L. Schwoebel, *Journal of Applied Physics*, 1969, **40**, 614-618.